THE ROYAL SOCIETY

Ultrafast near-field spectroscopy of single semiconductor quantum dots

By Christoph Lienau

Max-Born Institut für Nichtlineare Optik und Kurzzeitspektroskopie,
Max Born Straße 2A, 12489 Berlin, Germany (lienau@mbi-berlin.de)

Excitonic and spin excitations of single semiconductor quantum dots (QDs) currently attract attention as possible candidates for solid-state-based implementations of quantum logic devices. Due to their rather short decoherence times in the picosecond to nanosecond range, such implementations rely on using ultrafast optical pulses to probe and control coherent polarizations. We combine ultrafast spectroscopy and near-field microscopy to probe the nonlinear optical response of a *single* QD on a femtosecond time-scale. Transient reflectivity spectra show pronounced oscillations around the QD exciton line. These oscillations reflect phase-disturbing Coulomb interactions between the excitonic QD polarization and continuum excitations. The results show that although semiconductor QDs resemble in many respects atomic systems, Coulomb many-body interactions can contribute significantly to their optical nonlinearities on ultrashort time-scales.

Keywords: ultrafast spectroscopy; near-field microscopy; quantum dots;
optical nonlinearities; semiconductor nanostructures

1. Introduction

Our insight into the structure, function and dynamics of atomic, molecular, biological and solid-state nanostructures has been influenced strongly during the last two decades by two complementary and novel experimental tools, i.e. by scanning probe microscopy and ultrafast optics. The techniques of scanning probe microscopy (Wiesendanger 1998), in particular scanning tunnelling microscopy (STM) and atomic force microscopy (AFM), enable one to image the structure of surfaces on an atomic and even sub-atomic (Giessibl *et al*. 2000) scale, and give information about the local electronic density of states. STM techniques offer the unique ability to manipulate the position of single atoms with sub-nanometre precision and to assemble new structures on a nanoscale (Eigler & Schweizer 1990; Manoharan *et al*. 2000). Dynamic processes on surfaces, however, can only be studied on a time-scale given by the mechanical scan speed of the raster probe, i.e. typically on a millisecond time-scale.

Optical techniques, on the other hand, are inherently diffraction limited in spatial resolution to the scale of the wavelength of the light, i.e. to *ca.* 0.5 μm in the visible range. In combination with ultrashort light pulses, optics allows us to probe

structural changes on femtosecond time-scales. This makes ultrafast spectroscopy a unique tool for probing the elementary dynamics of electronic and nuclear motion in atomic, molecular and solid-state systems. It is the ideal technique for the time-resolved study of chemical-reaction dynamics (Fleming 1986; Zewail 2000) and the dynamics of electronic excitations in solid-state media (Shah 1998).

A particularly interesting research perspective lies in a combination of scanning probe microscopy and ultrafast optics to spatially resolve the ultrafast dynamics of optical excitations on ultrashort, nanometre length-scales. During the last decade, scientists have embarked on different strategies to attain this goal. The combination of a scanning tunnelling microscope with ultrashort light pulses offers ultimate, nanometre spatial resolution, yet, experimentally, has so far proven difficult (Gerstner *et al.* 2000*a*,*b*). An alternative concept relies on using the nano-optical techniques that have been developed during the last decade, e.g. aperture-based (Betzig & Trautman 1992; Lienau & Elsaesser 2000; Paesler & Moyer 1996) or apertureless scattering-type (Hillenbrand *et al.* 2002; Knoll & Keilmann 1999; Zenhausern *et al.* 1995) near-field microscopy, to break the diffraction limit and localize ultrashort light pulses to spatial dimensions of the order of 10–100 nm. Ultrafast nano-optics is currently a rapidly expanding field of research, as the newly developed experimental tools have the potential to probe and manipulate the dynamics of optical excitations of single nanostructures (Bonadeo *et al.* 1998*a*,*b*; Guenther *et al.* 2002; Stievater *et al.* 2001). This allows us to eliminate ensemble averaging, so far unavoidable in conventional far-field ultrafast experiments.

It is the aim of this review article to introduce a novel experimental approach combining near-field optics and femtosecond pump–probe spectroscopy to probe the nonlinear optical response of single nanostructures on ultrafast time-scales. This technique is implemented to study the coherent polarization dynamics and optical nonlinearity of a single semiconductor quantum dot (QD). Analysing transient reflectivity spectra, we directly demonstrate the effects of many-body Coulomb interactions on the excitonic polarization dynamics. The paper is organized as follows. In § 2, the experimental techniques applied in this study are introduced. Section 3 summarizes briefly some basic properties of interface QDs. The experimental results and their analysis are presented in § 4. A summary and some conclusions are given in § 5.

2. Ultrafast nanospectroscopy

A prerequisite for probing the dynamics of optical excitations on a nanometre scale in real space is the ability to generate and/or probe light spots with a temporal duration in the femtosecond range and nanometre spot sizes. A straightforward approach relies on transmitting ultrafast lasers through nanometre-sized apertures in non-transparent metal films. In the direct vicinity of the aperture, i.e. in its near field, the spatial resolution is defined by the dimension of the aperture, rather than by diffraction. The resolution can thus be increased by sufficiently decreasing the size of the aperture. If the aperture is fabricated at the tip of, for example, a metal-coated tapered optical fibre, it can be raster-scanned across the sample surface, using conventional techniques of scanning probe microscopy (Wiesendanger 1998). Near-field optical images are then generated by recording the transmitted or reflected light as a function of tip position. This approach is illustrated in figure 1. It depicts
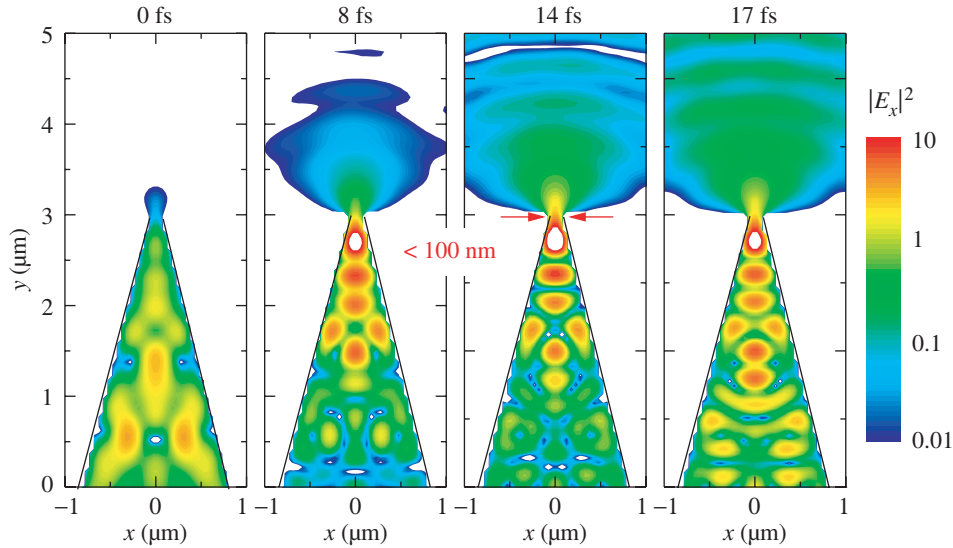
Figure 1. 2D FDTD simulation of the spatiotemporal evolution of a 10 fs light pulse at a centre wavelength of 810 nm propagating through a tapered, metalized fibre probe of 100 nm aperture diameter. The field intensity $|E_x(x, y, t)|^2$ is displayed on a logarithmic intensity scale at four different instants in time. Around $t = 14$ fs the pulse centre reaches the aperture, generating an ultrashort near-field light spot directly below the aperture. Note the strong back reflection of the pulse inside the fibre. The metal coating is assumed to be a perfect conductor.

a two-dimensional (2D) finite-difference time-domain (FDTD) simulation (Kunz & Lübbers 1993) of the propagation of a 10 fs light pulse with a centre wavelength of 810 nm through a metal-coated near-field fibre probe with a 100 nm aperture diameter (Müller & Lienau 2000). The spatial distribution of the field intensity $|E_x(x, z)|^2$ is shown on a logarithmic scale at four different instants in time. Around $t = 14$ fs the pulse centre reaches the aperture. A near-field light spot with a lateral dimension given by the aperture size is generated directly below the aperture. For a 100 nm aperture, its energy is about three orders of magnitude smaller than that of the incident pulse coupled into the fibre taper and this energy decreases strongly with decreasing aperture size. With current technology, aperture sizes down to *ca.* 30–40 nm can be fabricated, but the transmission coefficient is typically less than 10^{-4} (Matsuda *et al.* 2002; Naber *et al.* 2002).

In designing high spatial resolution experiments on semiconductor nanostructures, it is important that high optical quality semiconductor quantum wells (QWs), wires (QWRs) and dots are often buried at a depth of 50–100 nm below the sample surface in order to avoid non-radiative recombination effects. Thus, even if an ideal point-like dipole source was used, the spatial resolution would be limited to about 1.25–2.00 times the depth, i.e. to *ca.* 65–200 nm, depending on the polarization directions (Grober *et al.* 1999). This also means that the amplitude of the evanescent fields generated near the surface has decreased substantially when interacting with the buried semiconductor nanostructure.

Since many semiconductor nanostructures are grown on non-transparent substrates, using a reflection geometry is often desirable. In metal-coated tapers, however, most of the incident pulse energy is back-reflected inside the taper. This makes
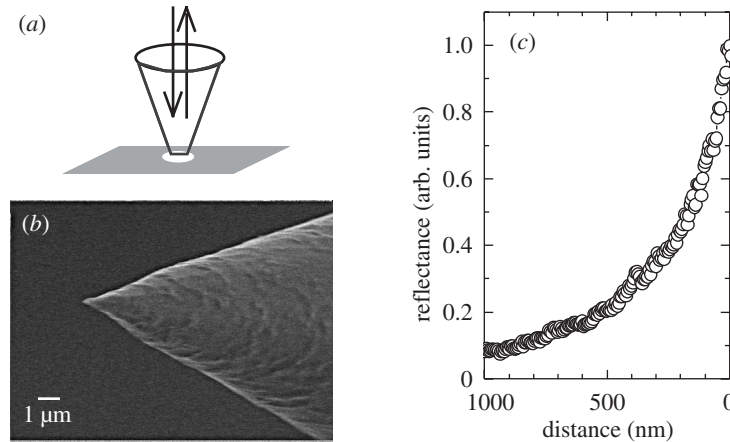
Figure 2. (*a*) Schematic of the illumination–collection mode. (*b*) SEM image of an etched uncoated near-field fibre probe. (*c*) Dependence of the reflected light detected in illumination–collection mode on the tip-to-sample distance.

it difficult to detect optical signals induced by the localized near-field light spot in a reflection geometry. Therefore, a slightly different approach is used in our experiments. We replace the metal-coated fibre probe by an uncoated, etched single-mode optical fibre taper with a cone angle of *ca.* 30°. Tube etching (Lambelet *et al.* 1998) is used to reduce the surface roughness and improve the optical quality of the taper (figure 2). These uncoated tips are used in an illumination–collection geometry (figure 2*a*), detecting the light that is reflected back into the taper. This detection geometry is particularly sensitive to the local surface reflectivity, as can be seen from the pronounced decrease of the reflected light intensity with increasing tip-to-sample distance (figure 2*c*). The reflected intensity decreases by a factor of 2 within the first 150 nm. An approximately exponential distance dependence, with a decay length of 250 nm free of interference oscillations, is observed for good quality tapers. Three-dimensional FDTD simulations (Müller & Lienau 2001) show that in the presence of a semiconductor almost all of the incident pulse energy is adiabatically guided into a spot at the very end of the taper, with a diameter of *ca.* 250 nm. In illumination–collection geometry, the spatial resolution is further improved, since the light passes twice through the aperture. It can reach less than 150 nm or about $\lambda/5$ (Intonti *et al.* 2001*a*). The FDTD simulations also show that a large fraction of the locally reflected light is coupled back into the tapered fibre. Experimentally we find that for GaAs samples, *ca.* 1% of the light coupled into the fibre is collected in this geometry. This high transmission and collection efficiency makes such uncoated fibre probes particularly well suited for semiconductor nanospectroscopy. Also, due to its pronounced distance dependence, the intensity of the locally reflected light can be used to sensitively sense the tip-to-sample distance with an accuracy of ± 2 nm. In our experiments the reflected light is used for a sensitive, contact-free distance regulation set-up, avoiding the mechanical strain that is sometimes found in shear-force-based feedbacks (Robinson *et al.* 1998).

When using these tapered fibre probes for femtosecond time-resolved spectroscopy, the temporal broadening of light pulses during propagation due to group-velocity dispersion (GVD) has to be considered. For a bandwidth-limited Gaussian input pulse
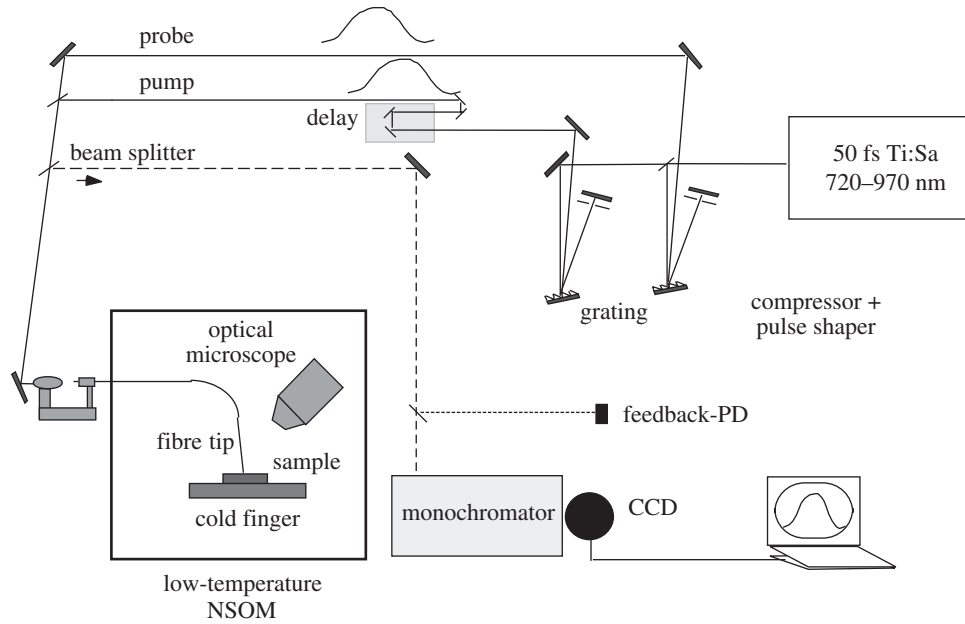
Figure 3. Schematic set-up of the near-field pump–probe spectrometer (Guenther *et al.* 1999; Lienau & Elsaesser 2000). Pump and probe pulses are derived from a 50 fs, 80 MHz repetition rate Ti:sapphire oscillator. The pulses are spectrally and temporally shaped in two independent compressor units in order to reach less than 200 fs time resolution at the exit of the fibre tip. In the illumination–collection-mode, pump and probe pulses are coupled into a near-field fibre probe and the reflected light is collected through the same fibre, spectrally dispersed in a monochromator and detected with a charge-coupled device (CCD) camera. The fibre probe is raster-scanned across the sample, which is mounted on the cold finger of a helium flow cryostat (Behme *et al.* 1997).

of duration τ_{in}, the output pulse length τ_{out} after propagation through a dispersive material of length L is given by $\tau_{\mathrm{out}} = \tau_{\mathrm{in}}\sqrt{1 + 4|k_{\mathrm{d}}|^2 L^2/\tau_{\mathrm{in}}^4}$. The GVD parameter $k_{\mathrm{d}} = \partial^2 k/\partial\omega^2$, with k being the wavevector and ω the angular frequency. Higher-order dispersion is neglected in this formula. For quartz single-mode fibres at a laser wavelength of *ca.* 800 nm, $k_{\mathrm{d}} \simeq 100\ \mathrm{ps}^2\ \mathrm{km}^{-1}$. In a typical, 100 cm long quartz single-mode fibre, a 50 fs input pulse is stretched to *ca.* 4 ps. Thus, a GVD precompensation set-up must be introduced before the fibre in order to add a negative GVD that compensates the positive GVD of the fibre. We use a grating compressor (Martinez 1987) (figure 3) and typically achieve a time resolution of less than 100 fs for a 40 cm long fibre taper and less than 200 fs for 100 cm long fibres. The achieved time resolution is mainly limited by higher-order dispersion inside the optical fibre, which cannot be compensated with this grating compressor. With unamplified laser pulses taken from mode-locked oscillators, the distortion of the pulse spectrum due to self-phase modulation is generally negligible.

A schematic of the near-field pump–probe set-up used in our experiments is shown in figure 3. Both pump and probe pulses are derived from a mode-locked Ti:sapphire oscillator providing pulses with a length of *ca.* 50 fs that are tunable in the wavelength range from 810 to 870 nm. The laser works at a repetition rate of 80 MHz and gives an average power of up to several hundreds of milliwatts. The laser output is split
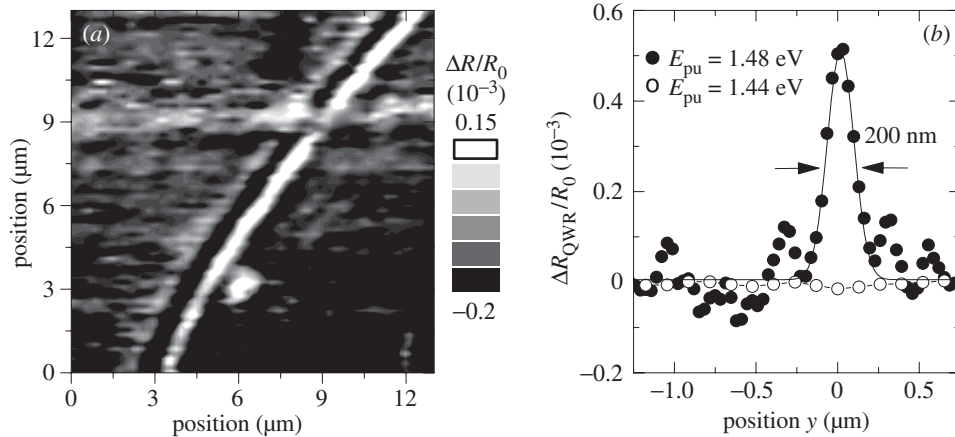
Figure 4. (*a*) Spatial map of the nonlinear pump-induced change in reflectivity of a single GaAs QWR. The map is recorded at room temperature with a probe laser set to 1.45 eV at the centre of the QWR absorption resonance. A pump laser at 1.52 eV generates electron–hole pairs in the QW surrounding the QWR. Trapping of carriers into the QWR bleaches the QWR absorption and decreases the reflectivity. (*b*) Spatial variation of the change in reflectivity along a line perpendicular to the QWR axis at a probe energy of 1.46 eV. The closed circles show data for resonant QWR excitation with a pump laser at $E_{pu} = 1.48$ eV, demonstrating 200 nm spatial resolution. For off-resonant excitation at $E_{pu} = 1.44$ eV the nonlinear signal vanishes (open circles).

into a pump and a probe beam. Each of these beams travels through a separate grating set-up for spectral selection and precompensation of GVD. Both pump and probe pulses are coupled into an uncoated near-field fibre probe. The probe light reflected from the sample is locally collected through the same fibre. The sample is mounted on the cold finger of a helium flow cryostat (Behme *et al*. 1997). For spectrally resolved pump–probe experiments, the collected light is dispersed in a 0.5 m monochromator yielding a spectral resolution of 60 µeV. The experiments are performed at low probe-laser powers of only *ca*. 100 nW coupled into the near-field fibre, requiring a high detection sensitivity. The collected light is therefore detected with a high-sensitivity liquid-nitrogen-cooled CCD camera. The signal-to-noise ratio of the CCD detection used in this set-up is approximately two times higher than the shot noise limit.

The spatial resolution that is obtained with this near-field pump–probe set-up is illustrated in figure 4, showing a spatial map of the nonlinear pump-laser-induced change in reflectivity of a single GaAs QWR (Guenther *et al*. 1999). The map is recorded at room temperature using a 100 fs probe laser pulse with a photon energy of 1.45 eV, the centre of the QWR absorption resonance. A pump-laser pulse, arriving 10 ps before the probe laser, generates electron–hole pairs in the QW surrounding the QWR. Trapping of carriers into the QWR bleaches the QWR absorption and thus decreases the reflectivity. The local pump-induced change in QWR reflectivity is clearly resolved in figure 4*a*. The temporal dynamics of the QWR reflectivity reveal an ultrafast trapping of carriers into the QWR (Guenther *et al*. 1999) and allow the time resolution of the optically induced non-equilibrium carrier transport along the QWR (Emiliani *et al*. 2000).
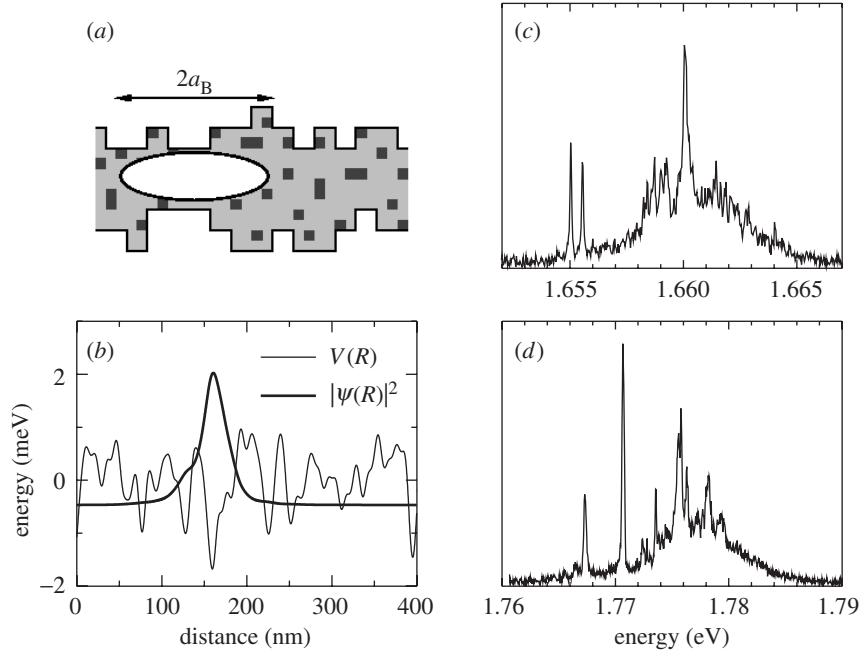
Figure 5. (*a*) Disorder in QWs arises from spatial fluctuations of the local QW thickness (interface roughness) and of the QW composition (alloy disorder). (*b*) Schematic of the effective disorder potential $V(\mathbf{R})$ and of a localized excitonic centre-of-mass wave function $|\Psi(\mathbf{R})|^2$. Representative near-field PL spectra ($T = 12$ K) of (*c*) a 5.1 nm thick and (*d*) a 3.3 nm thick (100) GaAs QW.

3. Interface QDs

Important QD model systems are thin semiconductor QWs. In such QWs, local monolayer height fluctuations at the interfaces (interface roughness) and fluctuations of the alloy composition (alloy disorder) are unavoidable (figure 5*a*). The resulting disordered potential leads to the localization of excitons in single 'interface' QDs with a confinement energy of *ca.* 10 meV (figure 5*b*). This disorder gives rise to a pronounced inhomogeneous broadening of far-field optical spectra. In experiments with high spatial and spectral resolution, however, the smooth, inhomogeneously broadened photoluminescence (PL) spectra break up into narrow emission spikes from a few localized excitons (Brunner *et al.* 1994; Emiliani 2001; Gammon *et al.* 1996*b*; Hess *et al.* 1994; Intonti *et al.* 2001*a*,*b*). This makes nano-optical techniques with high spectral resolution particularly well suited for studies of single QDs.

The linear optical properties of interface QDs resemble in many aspects those of atomic systems. At low temperatures, the excitonic lines display a narrow homogeneous linewidth of 30–50 µeV, in agreement with measured dephasing times of 20–30 ps. The QDs show a discrete absorption spectrum (Gammon *et al.* 1996*b*) and a fine structure splitting due to the spatial asymmetry of the monolayer islands. The temperature dependence of the exciton linewidth and the fine structure of these emission lines has been thoroughly investigated (Gammon *et al.* 1996*a*,*b*). The centre-of-mass wave function of localized excitons in interface QDs typically extends over several tens of nanometres. This results in large QD dipole moments of 50–100 D

and a particularly strong coupling of these excitons to light (Guest *et al.* 2002; Thränhardt *et al.* 2002). This makes interface QDs a particularly interesting model system for nonlinear spectroscopy of single QDs.

Detailed information about the underlying disorder potential and about the localization length of the excitonic wave functions is obtained from a statistical analysis of the autocorrelation function of such near-field spectra (Intonti *et al.* 2001*b*; von Freymann *et al.* 2002). Specifically, such experiments reveal excitonic-level repulsion as a robust correlation between localized exciton states with spatially overlapping wave functions, and allow us to estimate the correlation length of the underlying disorder potential.

In this work we investigate a sample consisting of 12 single QW layers of different thicknesses grown on a (100) GaAs substrate. The QW layers are separated by AlAs/GaAs short-period superlattice barriers, each formed by nine AlAs and GaAs layers with a total thickness of 23.8 nm. Here, we investigate the top seven QWs with thicknesses of 3.3–7.1 nm. The layers are buried at distances between 40 and 211 nm below the surface (figure 7). Growth interruptions of 10 s at each interface lead to a large correlation length of the QW disorder potential and to the formation of interface QDs. The growth interruptions are kept short in order to avoid a monolayer splitting of the macroscopic PL spectra, and to minimize the incorporation of impurities at the interfaces.

In figure 5*c,d* representative low-temperature ($T = 12$ K) near-field PL spectra are shown for the 3.3 and 5.1 nm thick (100) GaAs QWs. The spectra reveal clearly the emission from excitons localized in interface QDs. The linewidth of the sharp resonances is limited by the spectral resolution of 100 μeV. The spectra are recorded at a power of 110 nW, corresponding to an average excitation density well below one exciton per monolayer island. For excitation powers between 1 and 500 nW, we find a linear intensity dependence and an excitation-independent shape of the emission spectra, indicating negligible contributions from biexcitons and charged excitons. In addition to the sharp localized exciton emission, these spectra display a spectrally broad background emission from more delocalized excitons in QW continuum states (Intonti *et al.* 2001*a*).

4. Ultrafast nonlinear optical response of single QDs

The nonlinear optical properties of excitons in single-interface QDs have been investigated mainly by high-resolution nonlinear spectroscopy in the frequency domain (Bonadeo *et al.* 1998*a,b*). The third-order nonlinear response has been explained on the basis of homogeneously broadened two-level systems, in analogy to descriptions of atomic systems. On the other hand, it is well known that Coulomb interactions play an important role for ultrafast optical nonlinearities of higher-dimensional systems, such as QWs and QWRs. This raises the question of how transient many-body interactions arising from multiexcitonic interactions (Chen *et al.* 2001) and/or non-resonant optical excitations of the QD and its environment (for example, neighbouring QDs (Biolatti *et al.* 2000)) affect the QD optical nonlinearities and their ultrafast dynamics. Since such couplings are difficult to probe and/or control in ensembles, time-resolved studies of single QD nonlinearities are desirable.

Knowledge about the effects of many-body interactions on the optical nonlinearities of single QDs is particularly important in the light of recent proposals to use

excitonic excitations of single QDs as basic building blocks for quantum information processing in solids (Biolatti *et al.* 2000; Chen *et al.* 2001). Since the decoherence times of excitonic excitations are comparatively short, in the range of 10 ps to 1 ns (Borri *et al.* 2001), such implementations rely on controlling excitonic nonlinearities on an ultrafast, femtosecond time-scale, much shorter than the excitonic decoherence time. Controlled many-body interactions, e.g. via dipole–dipole coupling (Biolatti *et al.* 2000), are essential for coupling excitons in neighbouring QDs, i.e. for implementing controlled quantum gates. Uncontrolled many-body interactions with carriers in the environment of the QD, on the other hand, effectively couple the QD excitons to a surrounding bath and thus may be an important source of decoherence.

Here, the first femtosecond study of the nonlinear optical response of a single QD is reported. By analysing transient reflectivity spectra from single QDs, we directly probe the dynamics of the coherent excitonic polarization in the presence of non-equilibrium carriers excited in the environment of the QD. We show that excitation-induced dephasing by Coulomb interactions with continuum excitations is the dominant nonlinearity of the QD exciton on an ultrafast time-scale. This presents an important step forward in probing and manipulating coherent QD polarizations, which is of fundamental importance for semiconductor-based implementations of quantum information processing.

In this section we first describe how QD nonlinearities are probed in near-field reflectivity measurements and then analyse the dynamics of the QD nonlinearities. From these experiments, the radiative recombination rate of different QDs is extracted and their dipole moment is inferred. Then, the dynamics of the QD polarization in the presence of non-equilibrium carriers are discussed and excitation-induced dephasing is identified as the dominant QD nonlinearity on an ultrafast time-scale.

(*a*) *Near-field reflectivity spectra from single QDs*

In our experiments we probe the QD nonlinearity by measuring the spectrum of a probe laser locally reflected from the QD sample. Here, the effect of the excitonic QD polarization on the detected spectrum, i.e. the generation of the nonlinear reflectivity signal, is described.

Our experimental concept is outlined in figure 6a. A spectrally broad femtosecond laser, centred around the QW absorption, is coupled into the near-field fibre probe. The probe-laser light reflected from the sample is collected by the same fibre probe, dispersed in the monochromator and detected with the CCD camera. The spectrum of the femtosecond probe laser is typically 10 meV broad and thus much broader than the width of the individual exciton resonances (typically less than 100 μm). The steady-state reflectivity spectrum $R_0(\omega_{\text{det}})$ of the probe laser contains different weak spectrally narrow resonances from single QD transitions (figure 6a). A second, blue-shifted pump laser creates carriers in QW continuum states. This non-equilibrium carrier concentration affects the QD spectrum and thus gives rise to a modified probe reflectivity $R(\omega_{\text{det}})$. Differential probe reflectivity spectra

$$\frac{\Delta R(\omega_{\text{det}}, \Delta t)}{R_0} = \frac{R(\omega_{\text{det}}, \Delta t) - R_0(\omega_{\text{det}})}{R_0(\omega_{\text{det}})}$$

are recorded at a fixed spatial position of the near-field tip as a function of the time delay Δt between pump and probe pulses. From these, transient-differential
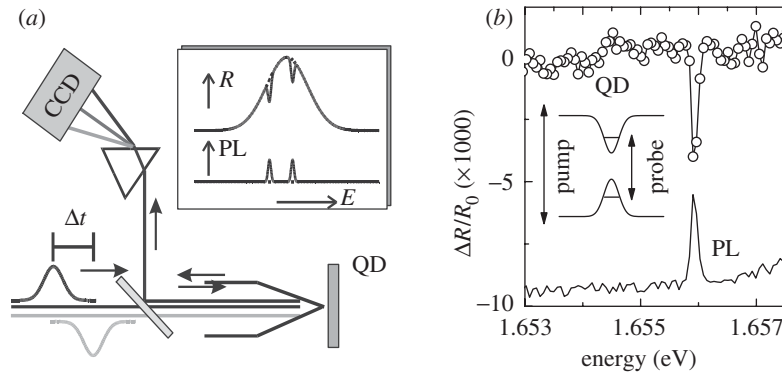
Figure 6. (*a*) Schematic of the experimental set-up and of near-field PL and reflectivity spectra of the QD sample. The reflectivity spectra measure the pump-induced change in the intensity of the femtosecond probe laser reflected from the QD sample. The probe laser is collected through the near-field probe, spectrally dispersed in a monochromator and detected with a CCD camera. (*b*) Near-field PL spectrum of a single QD (solid line) and differential reflectivity spectrum $\Delta R/R_0$ at $\Delta t = 30$ ps. PL and ΔR are recorded with identical pump pulses centred at 1.675 eV, exciting electron–hole pairs in 2D continuum states. The 100 nW probe pulses of 19 meV bandwidth are centred at 1.655 eV, around the QD absorption resonance. Inset: schematic energy diagram.

reflectivity-spectra information about the dynamics of the excitonic QD polarization is deduced. To probe the nonlinear optical response from single QDs, the high spatial resolution of the near-field technique is needed for two reasons. First, the combined spatial and spectral resolution allows the isolation of single QD resonances (figure 5). Second, the relative amplitude of the QD resonance in $R_0(\omega_{\text{det}})$ is, to a first approximation, inversely proportional to the square of the spatial resolution. Thus, improving the resolution from 1 µm to 100 nm increases the weak nonlinear QD signal by two orders of magnitude.

Specifically, in our experiments pump pulses centred at 1.675 eV with an energy of 1.5 fJ and a repetition rate of 80 MHz create less than five electron–hole pairs in QW states, corresponding to an excitation density of 5×10^9 cm^{-2}. The 1 fJ probe pulses of 18 meV bandwidth are centred at 1.655 eV, around the QW absorption resonance. Figure 6*b* depicts a differential reflectivity spectrum $\Delta R(E_{\text{det}})$ at a time delay of 30 ps in the low-energy region of the 5.1 nm QW absorption spectrum. It displays a single, spectrally sharp resonance at exactly the same spectral position E_{QD} as the simultaneously recorded near-field PL spectrum. The large amplitude of the signal of 5×10^{-3} is consistent with a spatial resolution of the experiment of 200–250 nm. 2D spatial scans indicate a resolution of 230 nm, limited by the QW-to-surface distance.

Figure 7 compares differential reflectivity $\Delta R(E_{\text{det}})$ and PL spectra recorded under similar excitation conditions for single localized excitons in five different QWs buried at distances of 95–211 nm below the surface. We very clearly observe a transition between a dispersion-like and an absorption-like line shape as the QW to surface distance is varied. This behaviour of the QD line shape can be understood in the framework of a local oscillator model as caused by the interference between the electric probe laser field $E_{\text{R}}(t)$ reflected from the sample surface and the field $E_{\text{QD}}(t)$ emitted from the QD in the back direction. A fraction $E_{\text{R}}(t)$ of the probe laser is
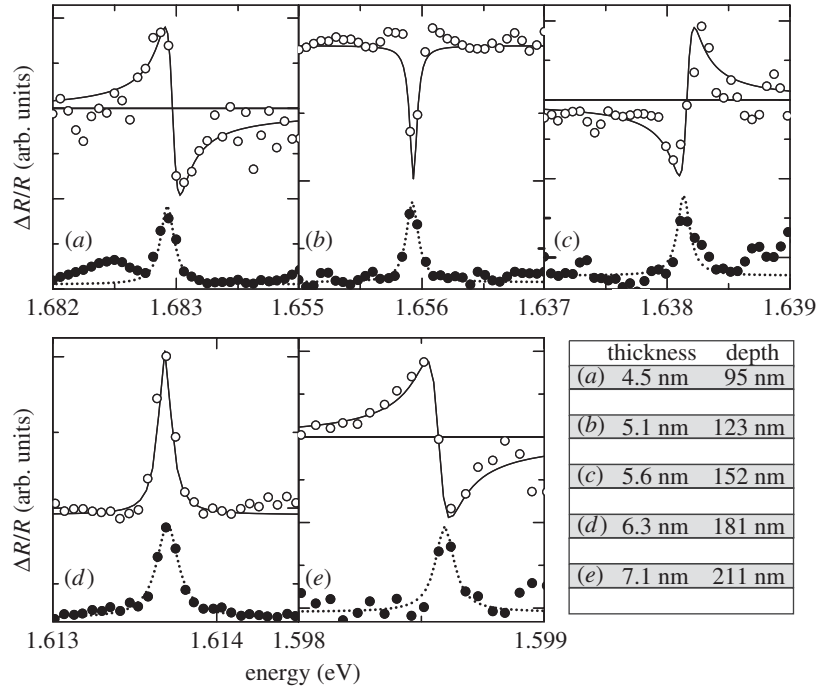
Figure 7. Differential reflectivity spectra (open circles) of five interface QDs located at different depths of 95–210 nm below the sample surface (see inset). The differential reflectivity spectra are compared with simultaneously recorded PL spectra. Note the transition between dispersive and absorptive line shapes.

reflected from the sample surface and coupled back into the near-field fibre probe. The probe field $E_T(t)$, transmitted into the semiconductor, induces a polarization

$$P_{QD}(t) = \int dt' \, \chi_{QD}(t') E_T(t - t')$$

of the QD located at a distance d below the sample surface. Here, $E_T(t)$ and χ_{QD} denote the probe field interacting with the QD and the QD susceptibility, respectively. The QD polarization re-emits an electric field, and a fraction of this field $E_{QD}(t)$ is locally collected by the near-field probe, where it interferes with $E_R(t)$. The time-integrated reflectivity $R(\omega)$ detected behind the monochromator is proportional to

$$|\tilde{E}_{QD}(\omega) + \tilde{E}_R(\omega)|^2 \simeq |\tilde{E}_R(\omega)|^2 + 2\operatorname{Re}[\tilde{E}_R^*(\omega)\tilde{E}_{QD}(\omega)],$$

where $\tilde{E}(\omega)$ denotes the Fourier transform of the field $E(t)$. Here, the finite monochromator resolution and the weak contribution from $|E_{QD}|^2$ has been neglected. Excitation by the pump laser affects the QD polarization and thus results in a change of the QD reflectivity. The differential reflectivity $\Delta R(\omega, \Delta t)$ represents the spectral interferogram of $\tilde{E}_R$ and $\tilde{E}_{QD}$:

$$\Delta R(\omega, \Delta t) \propto \operatorname{Re}\{\tilde{E}_R^*(\omega)[\tilde{E}_{QD}(\omega, \Delta t) - \tilde{E}_{QD,0}(\omega)]\}. \qquad (4.1)$$

The spectral shape of this interferogram evidently depends on the QD polarization dynamics and on the phase delay between $E_{QD}(t)$ and $E_R(t)$. Treating the QD for
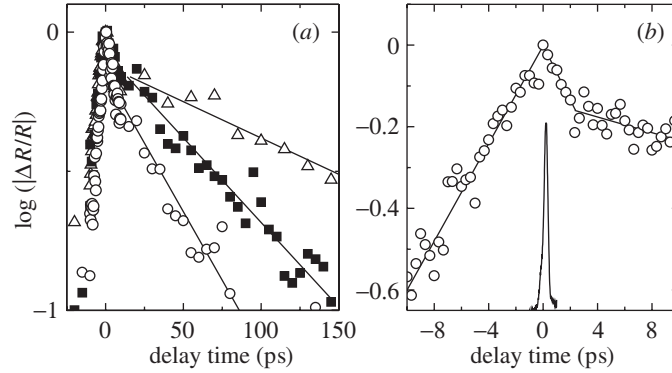
Figure 8. (*a*) Temporal dynamics of $\Delta R/R$ for three different QD resonances at 1.6598 eV (circles), 1.6614 eV (triangles) and 1.6648 eV (squares). The dynamics are displayed on a logarithmic ordinate scale. All decays are biexponential with a slow decay time varying between 30 and 150 ps. (*b*) Early time $\Delta R/R_0$ dynamics of a single QD resonance. A slow rise of $\Delta R/R_0$ is observed at negative time delays. The time resolution of the experiment is 150 fs, as indicated by the cross-correlation measurement (solid line around $\Delta t = 0$).

simplicity as a point dipole and the near-field tip as a point-like emitter, the phase delay depends on the distance between QD and near-field tip. This interference effect is nicely seen in figure 7 and explains the transition between an absorptive (Lorentzian) line shape $L(\omega)$ and a dispersive line shape, proportional to the first derivative $\partial L(\omega)/\partial \omega$. Since the QDs are buried more than 50 nm below the surface, the near-field terms of the QD dipole emission can be neglected, since they decay on a typical length-scale of $\lambda/(2\pi n) \simeq 35$ nm ($n \simeq 3.5$, refractive index). Based on an optical path of $4\pi nd/\lambda$, we estimate a phase change of $\pi/2$ for a change in QD sample distance of 28 nm. This is in reasonable agreement with the results of figure 7. We consider this convincing evidence for the validity of the phenomenological local oscillator model described above. Clearly, a detailed analysis of these data using, for example, a Green function solution of Maxwell's equations for a realistic experimental geometry is desirable for a quantitative comparison between experiment and theory.

(*b*) *Exciton recombination in single QDs*

In this subsection the dynamics of the differential QD reflectivity spectra on a 100 ps time-scale are analysed. The data allow us to extract the exciton lifetime and infer the QD dipole moment. Figure 8*a* shows the time evolution of $\Delta R(E_{\mathrm{QD}})$ for three different QD resonances. ΔR displays a slow decay with time constants τ_{QD} of 50–150 ps. The lifetime is found to fluctuate from QD to QD. The overall trend is a decrease with increasing E_{QD}. A clear correlation between $1/\tau_{\mathrm{QD}}$ and the magnitude of ΔR is observed.

The nonlinearities observed at sufficiently long positive Δt are easily understood on the basis of a simple two-level model for the QD nonlinearity. The pump laser creates a non-equilibrium distribution of electron–hole pairs in QW continuum states. Subsequent trapping of these carriers gives rise to a bleaching of the QD absorption and a concomitant decrease of the QD absorption. Hence, the decay time of ΔR reflects the lifetime of the individual exciton state probed. Following an earlier con-

jecture (Gammon *et al.* 1996*b*), the QD population decay is mainly dominated by radiative recombination, i.e. $\tau_{\text{rad}} \simeq \tau_{\text{QD}}$. We can then estimate the dipole moment of the individual QDs using (Andreani *et al.* 1999; Thränhardt *et al.* 2002)

$$\frac{1}{\tau_{\text{rad}}} = n \frac{\omega^3 d_{\text{QD}}^2}{3\pi\epsilon_0\hbar c^3}. \tag{4.2}$$

We estimate dipole moments d_{QD} of 50–85 D for τ_{rad} between 150 and 50 ps. These values are in rather good agreement with previous estimates (Andreani *et al.* 1999; Stievater *et al.* 2001). They exceed those of atomic systems by more than an order of magnitude and reflect the large spatial extension of the exciton centre-of-mass wave function in these QDs. Near-field autocorrelation spectra indicate an exciton localization length of *ca.* 40–50 nm. Due to the statistical nature of the disorder potential, the exciton localization length and thus the dipole moment and radiative recombination rate vary quite strongly from QD to QD, as seen in figure 8*b*. Theoretical models of localized excitons in disordered QWs (Savona *et al.* 2002) yield comparable results.

(*c*) *Coherent QD polarization dynamics and excitation-induced dephasing*

In this subsection the dynamics of the QD reflectivity on a time-scale of a few picoseconds is discussed. After non-resonant femtosecond excitation of carriers in continuum states we observe, unlike in atomic systems, transient differential-reflectivity spectra with pronounced oscillatory structure around the QD exciton resonance. These oscillations reflect the perturbation of the free-induction decay of the coherent QD polarization by transient many-body interactions.

Figure 8*b* plots the dynamics of QD reflectivity-change time delays between -10 ps and $+10$ ps. The time evolution of $\Delta R(E_{\text{QD}}, \Delta t)$ shows an 8 ps rise at negative delay times, much slower than the 150 fs cross-correlation of pump and probe pulses. A biexponential decay is found at positive delays. The fast decay time of *ca.* 6 ps is similar for all different QDs investigated, whereas the decay time of the slow component varies from dot to dot. The reflectivity $\Delta R_t(\Delta t) = \int \mathrm{d}E_{\text{det}}\,\Delta R(E_{\text{det}}, \Delta t)$, spectrally integrated over an energy interval of 2 meV around the QD resonance, vanishes at negative delay times and shows a slow exponential decay at $\Delta t > 0$. The spectral characteristics of the differential reflectivity are markedly different at positive and negative delays (figure 9). At negative delays, pronounced spectrally symmetric oscillations around the excitonic resonance are observed. Their oscillation period decreases with increasing negative time delay. At large positive delays, the spectra show a bleaching of the QD resonance.

To account for this behaviour, one has to consistently describe the dynamics of the field $E_{\text{QD}}(t)$ radiated from the coherent QD polarization $P_{\text{QD}}(t)$. We phenomenologically describe the QD as an effective two-level system with a ground, no-exciton state $|0\rangle$, and an excited one-exciton state $|1\rangle$. Within the density-matrix formalism, $P_{\text{QD}}(t)$ is given as $P_{\text{QD}}(t) = d_{\text{QD}}^* \rho_{01} + \text{c.c.}$, where d_{QD} denotes the QD dipole moment and ρ_{01} the microscopic QD polarization (Haug & Koch 1994). Then, the well-known Bloch equations hold and ρ_{01} obeys the equation of motion

$$\frac{\partial}{\partial t}\rho_{01}(t) = -\mathrm{i}\omega_{\text{QD}}\rho_{01}(t) + \mathrm{i}(1 - 2n_{\text{QD}})\omega_{\text{R}} - \gamma\rho_{01}(t), \tag{4.3}$$
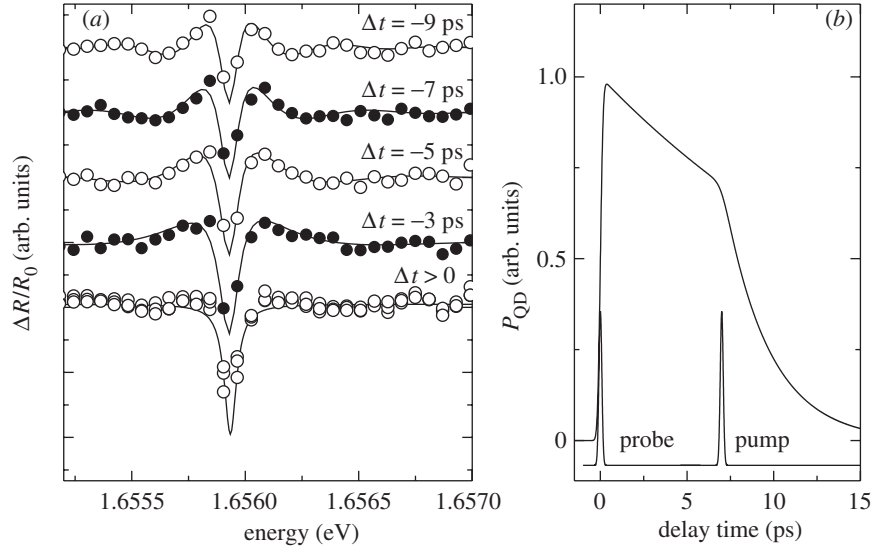
Figure 9. (*a*) Near-field $\Delta R/R_0$ spectra (circles) at different delay times Δt. The spectra at $\Delta t < 0$ display pronounced spectral oscillations around the excitonic resonance. The solid lines shows simulated spectra for the perturbed free-induction decay of the coherent QD polarization assuming $T_2 = 15$ ps. (*b*) Dynamics of $P_{\mathrm{QD}}(t)$ extracted from the time-dependent near-field $\Delta R/R_0$ spectra.

with exciton energy ω_{QD}, dephasing rate γ, exciton population n_{QD} and generalized Rabi frequency ω_{R}.

In the absence of a pump laser, the resonant probe laser impulsively excites a coherent QD polarization that then decays with the dephasing rate γ. The re-emitted field interferes with the reflected probe laser field, giving rise to a Lorentzian QD line shape in $R_0(\omega)$ (figure 6). The fact that we observe a linewidth that is limited by our monochromator resolution of *ca.* 60 µeV gives a lower limit for the QD dephasing time of $T_2 = 1/\gamma > 15$ ps.

Such a line shape is only observed under weak excitation conditions. For strong excitation, Rabi oscillations (Stievater *et al.* 2001; Zrenner *et al.* 2002) influence the polarization and population dynamics and affect the QD line shape. The experiments reported in this paper are all performed in the weak excitation limit with a probe pulse area of less than 0.4π. In additional experiments, which will be discussed elsewhere, clear Rabi oscillations are observed for resonant QD excitation and time-resolved detection of the induced biexcitonic QD nonlinearity.

The transient spectral oscillations around the QD exciton resonance at negative time delays indicate that this free-induction decay of the $P_{\mathrm{QD}}(t)$ is perturbed by the presence of the pump laser. In semiconductors, such oscillations have so far only been observed for higher-dimensional systems, e.g. studies of transient QW nonlinearities (Fluegel *et al.* 1987; Sokoloff *et al.* 1988). In our experiments, the off-resonant pump does not directly interact with the QD dipole but creates electron–hole pairs (density n_{QW}) in the QW continuum. Thus many-body interactions perturb the free-induction decay of $P_{\mathrm{QD}}(t)$.

The spectra at $\Delta t < 0$ are quantitatively described by assuming that an excitation-induced dephasing (Wang *et al.* 1993), i.e. an increase in γ due to the interaction

between ρ_{01} and n_{QW}, is the leading contribution to the QD nonlinearity at early times. Coulomb scattering between the QD dipole and the initial non-equilibrium carrier distribution in the QW causes this additional fast damping of ρ_{01}. In the frequency domain, this excitation-induced dephasing leads to oscillatory structures in the spectrum with a period determined by the time delay between probe and pump. The solid lines in figure 9a are calculated from (4.3) by assuming that the probe-induced QD polarization $P_{QD}(t)$ decays initially with an effective dephasing time $T_2 = 15$ ps, decreasing to $T_{EID} = 3$ ps after the arrival of the pump laser (figure 9b). Such an excitation-induced dephasing model accounts quantitatively for the transient oscillations and this analysis allows us to extract the QD polarization dynamics.

A detailed theoretical analysis of the data was performed on the basis of the semiconductor Bloch equations in the mean-field approximation (Guenther *et al.* 2002). In a first approximation, the excitation-induced dephasing rate should increase linearly with the pump-induced non-equilibrium carrier concentration n_{QW} in QW continuum states. Such a phenomenological model for the dephasing rate $\gamma = 1/T_2 + \gamma_1 n_{QW}$ was included in the simulations, and good agreement between experiment and theoretical simulation was obtained. The theoretical simulations clearly show the importance of excitation-induced dephasing to the perturbed free-induction decay.

The assumption of a density-dependent dephasing rate can also explain the fast decay of the differential reflectivity at early positive delay times (figure 8b). We assume that n_{QW} decays on a time-scale of *ca.* 3 ps. This decay is most likely due to carrier trapping into QD states. Then, the initial fast differential-reflectivity decay reflects the transition from a QD nonlinearity dominated by excitation-induced dephasing to a nonlinearity dominated by exciton bleaching due to the population relaxation into the QD. The slow decay of the differential reflectivity on a time-scale of tens of picoseconds then reflects the population lifetime, i.e. the electron–hole pair recombination time in the individual QDs. It is determined by radiative recombination and inversely proportional to the square of the QD dipole moment, as discussed above.

This model for the QD nonlinearity allows us to quantitatively describe the dynamics of the differential reflectivity at both positive and negative delay times (figure 10). It accounts for the transient spectral oscillations at negative delay times and reproduces the biexponential decay at positive delay times.

The experimental spectra probe the dynamics of the QD polarization $P_{QD}(t)$, which is given as the product of the dipole moment d_{QD} and the microscopic polarization ρ_{01}. Thus, one may speculate that a change in the oscillator-strength model of the QD may account for the observed spectra (Joffre 2003). Such an oscillator-strength model is inconsistent with our experimental results. Within such a model one expects an increase in $\Delta R(E_{QD}, \Delta t)$ at positive delay times on the time-scale of the switch-off time of the dipole moment (figure 10). In contrast an initial decay is observed, in agreement with the assumption of a nonlinearity that is dominated by excitation-induced dephasing.

These results show quite clearly that, although single QDs resemble atomic systems in many respects, Coulomb many-body interactions contribute significantly to their optical nonlinearities on ultrashort time-scales. Such many-body interactions have to be taken into account as important additional dephasing mechanisms. On the other hand, the now-established ability to probe the dynamics of coherent polariza-
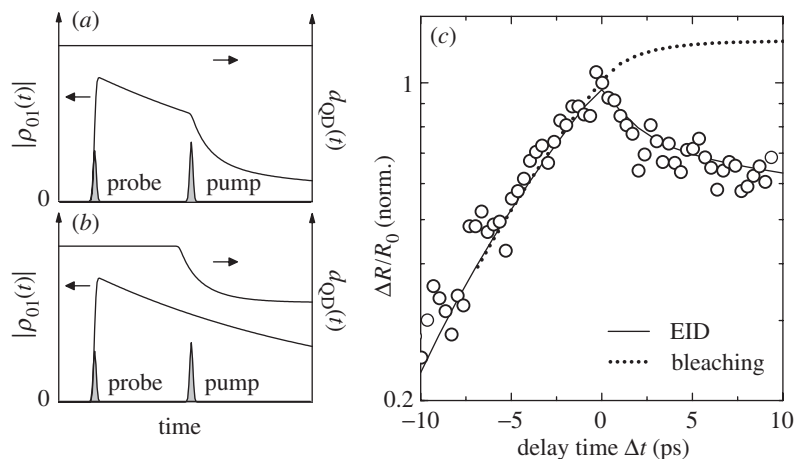
Figure 10. Illustration of two models assuming (*a*) excitation-induced dephasing and (*b*) bleaching as the dominant QD nonlinearity. (*c*) Experimental $\Delta R(\omega_{QD})/R_0$ dynamics and simulations based on the two models.

tion of single excitons in real time improves our understanding of such interactions. This is important for optimizing QD geometries and excitonic excitations with their environment.

Also, the strong Coulomb and light-matter interactions in excitonic systems open up new and very interesting ways for a controlled ultrafast manipulation of coherent QD polarizations, e.g. via dipole–dipole interactions of neighbouring QDs (Biolatti *et al.* 2000). This is highly relevant for semiconductor-based implementations of quantum information processing.

5. Conclusion

In summary we have described and demonstrated a novel experimental technique, combining near-field microscopy and femtosecond pump–probe spectroscopy, to probe the nonlinear optical response of single nanostructures. The techniques provide a spatial and temporal resolution of 200 nm and 100 fs, respectively. Detecting the spectrally resolved reflected-probe laser light with a high-sensitivity CCD camera allows the temporal resolution of the optical nonlinearity of a *single* semiconductor QD. The high sensitivity of the pump–probe technique demonstrated in this work makes it a powerful tool for probing nanoscale optical nonlinearities of a wide class of materials, e.g. organic semiconductors or photochromic molecules. It will be interesting to further improve the spatial resolution of the near-field pump–probe technique, e.g. by using apertureless metallic probes. This opens the way to performing nonlinear optical spectroscopy on a length-scale of 10 nm.

References

Andreani, L. C., Panzarini, G. & Gerard, J. M. 1999 Strong-coupling regime for quantum boxes in pillar microcavities: theory. *Phys. Rev.* B **60**, 13 276–13 279.

Behme, G., Richter, A., Süptitz, M. & Lienau, C. 1997 Vacuum near-field scanning optical microscope for variable cryogenic temperatures. *Rev. Scient. Instrum.* **68**, 3458–3465.

Betzig, E. & Trautman, J. K. 1992 Near-field optics: microscopy, spectroscopy and surface modification beyond the diffraction limit. *Science* **257**, 189–195.

Biolatti, E., Iotti, R., Zanardi, P. & Rossi, F. 2000 Quantum information processing with semiconductor macroatoms. *Phys. Rev. Lett.* **85**, 5647–5650.

Bonadeo, N. H., Chen, G., Gammon, D., Katzer, D. S., Park, D. & Steel, D. G. 1998*a* Nonlinear nano-optics: probing one exciton at a time. *Phys. Rev. Lett.* **81**, 2759–2762.

Bonadeo, N. H., Erland, J., Gammon, D., Park, D., Katzer, D. S. & Steel, D. G. 1998*b* Coherent optical control of the quantum state of a single quantum dot. *Science* **282**, 1473–1476.

Borri, P., Langbein, W., Schneider, S., Woggon, U., Sellin, R. L., Ouyang, D. & Bimberg, D. 2001 Ultralong dephasing time in InGaAs quantum dots. *Phys. Rev. Lett.* **87**, 157 401.

Brunner, K., Abstreiter, G., Böhm, G., Tränkle, G. & Weimann, G. 1994 Sharp-line photo-luminescence and two-photon absorption of zero-dimensional biexcitons in a GaAs/AlGaAs structure. *Phys. Rev. Lett.* **73**, 1138–1141.

Chen, P., Piermarocchi, C. & Sham, L. J. 2001 Control of exciton dynamics in nanodots for quantum operations. *Phys. Rev. Lett.* **87**, 067 401.

Eigler, D. M. & Schweizer, E. K. 1990 Positioning single atoms with a scanning tunnelling microscope. *Nature* **344**, 524–526.

Emiliani, V., Guenther, T., Lienau, C., Nötzel, R. & Ploog, K. H. 2000 Ultrafast near-field spectroscopy of quasi-one-dimensional transport in a single quantum wire. *Phys. Rev.* B **61**, R10 583–R10 586.

Emiliani, V., Intonti, F., Lienau, C., Elsaesser, T., Nötzel, R. & Ploog, K. H. 2001 Near-field optical imaging and spectroscopy of a coupled quantum wire-dot structure. *Phys. Rev.* B **64**, 155 316.

Fleming, G. R. 1986 *Chemical applications of ultrafast spectroscopy.* Oxford University Press.

Fluegel, B., Peyghambarian, N., Olbright, G., Lindberg, M., Koch, S. W., Joffre, M., Hulin, D., Migus, A. & Antonetti, A. 1987 Femtosecond studies of coherent transients in semiconductors. *Phys. Rev. Lett.* **59**, 2588–2591.

Gammon, D., Snow, E. S., Shanabook, B. V., Katzer, D. S. & Park, D. 1996*a* Homogeneous linewidths in the optical spectrum of a single gallium arsenide quantum dot. *Science* **273**, 87–90.

Gammon, D., Snow, E. S., Shanabrook, B. V., Katzer, D. S. & Park, D. 1996*b* Fine structure splitting in the optical spectra of single GaAs quantum dots. *Phys. Rev. Lett.* **76**, 3005–3008.

Gerstner, V., Knoll, A., Pfeiffer, W., Thon, A. & Gerber, G. 2000*a* Femtosecond laser-assisted scanning tunneling microscopy. *J. Appl. Phys.* **88**, 4851–4859.

Gerstner, V., Thon, A. & Pfeiffer, W. 2000*b* Thermal effects in pulsed laser-assisted scanning tunneling microscopy. *J. Appl. Phys.* **87**, 2574–2580.

Giessibl, F. J., Hembacher, S., Bielefeldt, H. & Mannhart, J. 2000 Subatomic features on the silicon (111)-(7*7) surface observed by atomic force microscopy. *Science* **289**, 422–425.

Grober, R. D., Rutherford, T. & Harris, T. D. 1996 Modal approximation for the electromagnetic field of a near-field optical probe. *Appl. Opt.* **35**, 3488–3495.

Guenther, T., Emiliani, V., Intonti, F., Lienau, C., Elsaesser, T., Nötzel, R. & Ploog, K. H. 1999 Femtosecond near-field spectroscopy of a single GaAs quantum wire. *Appl. Phys. Lett.* **75**, 3500–3502.

Guenther, T., Lienau, C., Elsaesser, T., Glanemann, M., Axt, V. M., Kuhn, T., Eshlaghi, S. & Wieck, A. D. 2002 Coherent nonlinear optical response of single quantum dots studied by ultrafast near-field spectroscopy. *Phys. Rev. Lett.* **89**, 057 401.

Guest, J. R. (and 11 others) 2002 Measurement of optical absorption by a single quantum dot exciton. *Phys. Rev.* B **65**, 241 310(R).

Haug, H. & Koch, S. W. 1994 *Quantum theory of the optical and electronic properties of semiconductors*, 2nd edn. Singapore: World Scientific.

Hess, H. F., Betzig, E., Harris, T. D., Pfeiffer, L. N. & West, K. W. 1994 Near-field spectroscopy of the quantum constituents of a luminescent system. *Science* **264**, 1740–1745.

Hillenbrand, R., Taubner, T. & Keilmann, F. 2002 Phonon-enhanced light–matter interaction at the nanometre scale. *Nature* **418**, 159–162.

Intonti, F., Emiliani, V., Lienau, C., Elsaesser, T., Nötzel, R. & Ploog, K. H. 2001*a* Near-field optical spectroscopy of localized and delocalized excitons in a single GaAs quantum wire. *Phys. Rev.* B **63**, 075 313.

Intonti, F., Emiliani, V., Lienau, C., Elsaesser, T., Savona, V., Runge, E., Zimmermann, R., Nötzel, R. & Ploog, K. H. 2001*b* Quantum mechanical repulsion of exciton levels in a disordered quantum well. *Phys. Rev. Lett.* **87**, 076 801.

Joffre, M. 2003 Comment on 'Coherent nonlinear optical response of single quantum dots studied by ultrafast near-field spectroscopy'. *Phys. Rev. Lett.* **90**, 139 701.

Knoll, B. & Keilmann, F. 1999 Near-field probing of vibrational absorption for chemical microscopy. *Nature* **418**, 134–137.

Kunz, K. S. & Lübbers, R. J. 1993 *The finite difference time domain method for electromagnetics.* Boca Raton, FL: CRC Press.

Lambelet, P., Sayah, A., Pfeffer, M., Philipona, C. & Marquis-Weible, F. 1998 Chemically etched fiber tips for near-field optical microscopy: a process for smoother tips. *Appl. Optics* **37**, 7289–7292.

Lienau, C. & Elsaesser, T. 2000 *Spatially and temporally resolved near-field scanning optical microscopy studies of semiconductor quantum wires.* Semiconductors and Semimetals, vol. 67, pp. 39–107.

Manoharan, H. C., Lutz, C. P. & Eigler, D. M. 2000 Quantum mirages formed by coherent projection of electronic structure. *Nature* **403**, 512–515.

Martinez, O. 1987 3000-times grating compressor with positive group velocity dispersion. *IEEE J. Quant. Electron.* **23**, 59–64.

Matsuda, K., Saiki, T., Nomura, S., Mihara, M. & Aoyagi, Y. 2002 Near-field photoluminescence imaging of single semiconductor quantum constituents with a spatial resolution of 30 nm. *Appl. Phys. Lett.* **81**, 2291–2293.

Müller, R. & Lienau, C. 2000 Propagation of femtosecond optical pulses through uncoated and metal-coated near-field fiber probes. *Appl. Phys. Lett.* **76**, 3367–3369.

Müller, R. & Lienau, C. 2001 Three-dimensional analysis of light propagation through uncoated near-field fibre probes. *J. Microsc.* **202**, 339–346.

Naber, A., Molenda, D., Fischer, U. C., Maas, H.-J., Höppener, C., Lu, N. & Fuchs, H. 2002 Enhanced light confinement in a near-field optical probe with a triangular aperture. *Phys. Rev. Lett.* **89**, 210 801.

Paesler, M. A. & Moyer, P. J. 1996 *Near-field optics.* Wiley.

Robinson, H. D., Müller, M. G., Goldberg, B. B. & Merz, J. L. 1998 *Appl. Phys. Lett.* **72**, 2081–2083.

Savona, V., Runge, E., Zimmermann, R., Intonti, F., Emiliani, V., Lienau, C. & Elsaesser, T. 2002 Level repulsion of localized excitons in disordered quantum wells. *Physica Status Solidi* A **190**, 625–629.

Shah, J. 1998 *Ultrafast spectroscopy of semiconductors and semiconductor nanostructures*, 2nd edn. Springer.

Sokoloff, J. P., Joffre, M., Fluegel, B., Hulin, D., Lindberg, M., Koch, S. W., Migus, A., Antonetti, A. & Peyghambarian, N. 1988 Transient oscillations in the vicinity of excitons and in the band of semiconductors. *Phys. Rev.* B **38**, 7615–7621.

Stievater, T. H., Li, X., Steel, D. G., Gammon, D., Katzer, D. S., Park, D., Piermarocchi, C. & Sham, L. J. 2001 Rabi oscillations of excitons in single quantum dots. *Phys. Rev. Lett.* **81**, 2759–2762.

Thränhardt, A., Ell, C., Khitrova, G. & Gibbs, H. M. 2002 Relation between dipole moment and radiative lifetime in interface quantum dots. *Phys. Rev.* B **65**, 035 327.

von Freymann, G., Neuberth, U., Deubel, M., Wegener, M., Khitrova, G. & Gibbs, H. M. 2002 Level repulsion in nanophotoluminescence spectra from single GaAs quantum wells. *Phys. Rev.* B **65**, 205 327.

Wang, H., Ferrio, K., Steel, D. G., Hu, Y. Z., Binder, R. & Koch, S. W. 1993 Transient nonlinear optical response from excitation-induced dephasing in GaAs. *Phys. Rev. Lett.* **71**, 1261–1264.

Wiesendanger, R. 1998 *Scanning probe microscopy.* Springer.

Zenhausern, F., Martin, Y. & Wickramasinghe, H. K. 1995 Scanning interferometric apertureless microscopy: optical imaging at 10 angstrom resolution. *Science* **269**, 1083–1085.

Zewail, A. H. 2000 Femtochemistry: atomic-scale dynamics of the chemical bond. *J. Phys. Chem.* A **104**, 5660–5694.

Zrenner, A., Beham, E., Stuffer, S., Findeis, F., Bichler, M. & Abstreiter, G. 2002 Coherent properties of a two-level system based on a quantum-dot photodiode. *Nature* **418**, 612–614.